International Journal of Nanomedicine

Dovepress
Taylor & Francis Group

Open Access Full Text Article

ORIGINAL RESEARCH

Comparative Evaluation of Nano-Assemblies From Shaoyao Gancao Decoction on Paeoniflorin Bioavailability

Chengying Shen[1], Xinling Wei[1,2], Chaoying Du[1], Shuangchen Zhang[2,3], Nianzhan Zhang[2,3], Pengfei Yue[2,3], Baode Shen[2,3]

[1]Department of Pharmacy, Jiangxi Provincial People's Hospital, the First Affiliated Hospital of Nanchang Medical College, Nanchang, Jiangxi, 330006, People's Republic of China; [2]Key Laboratory of Modern Preparation of Traditional Chinese Medicine, Ministry of Education, Jiangxi University of Chinese Medicine, Nanchang, Jiangxi, 330004, People's Republic of China; [3]State Key Laboratory for the Modernization of Classical and Famous Prescriptions of Chinese Medicine, Nanchang, Jiangxi, 330004, People's Republic of China

Correspondence: Pengfei Yue; Baode Shen, Key Laboratory of Modern Preparation of Traditional Chinese Medicine, Ministry of Education, Jiangxi University of Chinese Medicine, Nanchang, Jiangxi, 330004, People's Republic of China, Email ypfpharm@126.com; shenbaode@163.com

Purpose: The present study aimed to systematically compare the in vitro and in vivo characteristics of three nano-assemblies with different components derived from Shaoyao Gancao Decoction (SGD), with particular emphasis on their differential effects on oral absorption of paeoniflorin (Pae).

Methods: The self-assembled nanoparticles of SGD (SGD-SAN), glycyrrhizic acid self-assembled nanomicelles (GL-SNM), and Glycyrrhiza protein self-assembled nanoparticles (GP-SAN) were separated or prepared, and characterized in terms of particle size, zeta potential, morphology, drug loading, and in vitro release behavior. The single-pass intestinal perfusion and pharmacokinetic studies of SGD-SAN, GL-SNM, and GP-SAN following oral administration were performed to evaluate their absorption-enhancing effect. Chemical interference agents (NaCl, urea, and Tween 20) were added, followed by particle size detection, to identify the types of intermolecular forces in the self-assemblies.

Results: Three nano-assemblies exhibited significant differences in particle size (133 nm for SGD-SAN, 154 nm for GL-SNM, and 184 nm for GP-SAN) and drug loading (5.54% for SGD-SAN, 10.70% for Pae GL-SNM, and 21.52% for Pae GP-SAN). While hydrophobic interactions act as the common core force driving the formation of all nano-assemblies, their dependencies on other intermolecular forces vary remarkably. SGD-SAN, GL-SNM, and GP-SAN exhibited sustained Pae release (50–75% over 12 h vs 100% for the Pae solution in 2 h). In situ intestinal perfusion in rats showed significantly higher effective permeability coefficients (P_{eff}) for all nano-assemblies than the Pae solution, with GP-SAN exhibiting the highest ileal absorption, which may be attributed to preferential M-cell uptake facilitated by its protein-rich composition. Pharmacokinetic studies confirmed superior performance of GP-SAN with the highest AUC_{0-t} (11209.01 ± 2093.72 ng/mL·h) and C_{max} (2896.04 ± 255.01 ng/mL), representing 2.0-fold and 3.0-fold increases over Pae solution (5676.14 ± 311.61 ng/mL·h & 964.89 ± 128.81 ng/mL), respectively. GL-SNM and SGD-SAN also significantly enhanced the bioavailability (AUC_{0-t} increased by 65% and 45%, respectively).

Conclusion: These results suggested that nano-assemblies, particularly protein-based GP-SAN, provide a structural foundation for SGD's bioavailability-enhancing effect.

Keywords: shaoyao gancao decoction, nano assembly, oral absorption, paeoniflorin

Introduction

Shaoyao Gancao Decoction (SGD) is a famous traditional Chinese medicine (TCM) formula originating from the *Treatise on Febrile diseases* written by Zhongjing Zhang during the Han Dynasty.[1,2] It is composed of *Paeoniae Radix Alba* (PRA, called Baishao in China) and *Glycyrrhizae Radix et Rhizoma* (GRR, called Gancao in China) at a ratio of 1:1, and is widely used in the treatment of digestive system diseases and gynecological disorders.[2,3] Recent studies have demonstrated that SGD possesses multiple pharmacological effects, including spasmolysis, analgesia, and

Received: 3 June 2025
Accepted: 23 November 2025
Published: 2 December 2025

Graphical Abstract

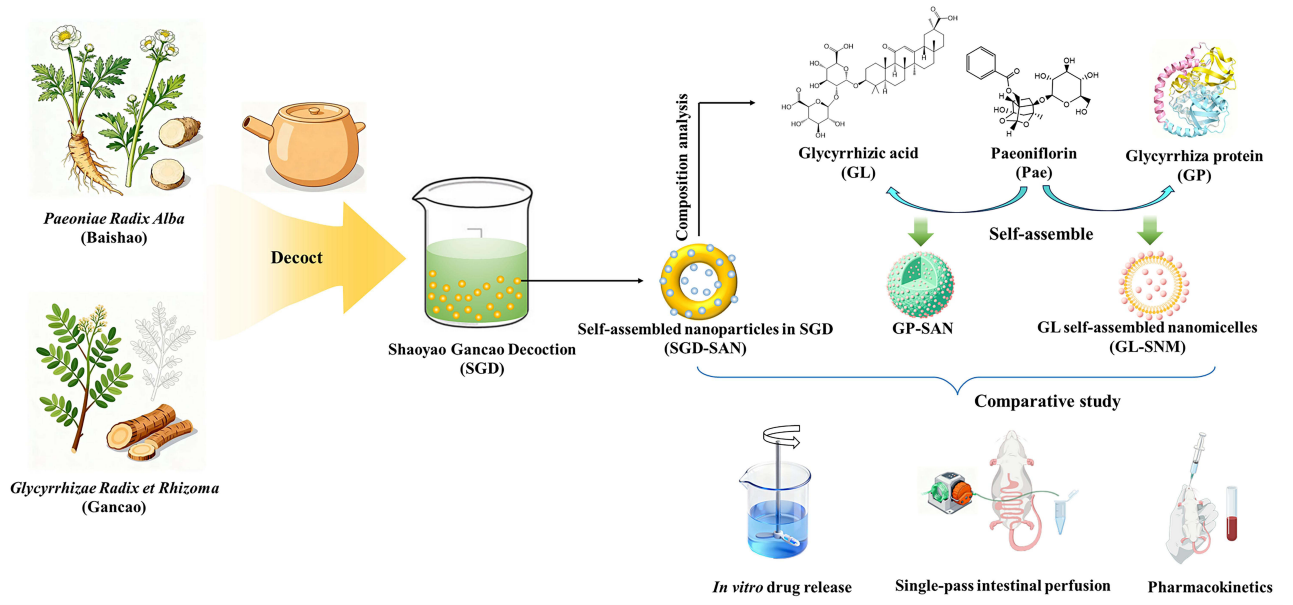

anti-inflammatory effects, and has various chemical components, including paeoniflorin (Pae), oxypaeoniflorin, albiflorin, benzoylpaeoniflorin, glycyrrhizic acid (GL), liquiritin apioside, liquiritin, liquiritigenin.[1–4] However, these components are predominantly glycosides or flavonoids, which exhibit poor oral bioavailability because of their high polarity or low solubility. In particular, Pae, a P-glycoprotein (P-gp) substrate, was demonstrated to be extremely poor absorption with absolute oral bioavailability ranging from 3% to 4%.[5,6]

Notably, TCM herbal formulas exhibit an intriguing characteristic that certain phytochemicals with inherently low bioavailability show dramatically increased absorption when orally administered with TCM formula decoctions. Representatively, the bioavailability of Pae was significantly improved by the oral administration of SGD,[7] but the mechanism underlying the bioavailability improvement remains unclear. There have been some studies on the potential mechanisms by which active ingredients of licorice affect Pae absorption. However, there are contradictory findings regarding the effects of licorice constituents on P-gp. Glycyrrhetinic acid (GA) and 18β-GA (a predominant conformation of GA) have shown P-gp inhibitory activity in certain studies.[8,9] In contrast, other studies have reported that GA activated the function and expression of P-gp.[10,11] Additionally, GL has been reported to decrease the absorption of Pae by inducing the activity of P-gp.[12] In another study, GL exhibited concentration-dependent effects on intestinal Pae absorption: 1 mM GL significantly increased absorption in the jejunum after 45 min and in the ileum after 90 min, whereas 100 μM GL inhibited absorption in the jejunum.[13] Therefore, the underlying mechanisms by which oral administration of SGD improves bioavailability of Pae remain to be elucidated due to these inconsistent findings.

Recently, self-assemblies of TCM, also known as supramolecules and natural nanoparticles, have received growing attention as they can not only help elaborate the scientific connotation of TCM compatibility, but also be used as drug carriers to improve the bioavailability and biological activities of medicinal components.[14–17] Self-assemblies in TCM decoctions, particularly in TCM formulas, result from high-temperature boiling-induced non-covalent interactions (hydrogen bonding, electrostatic forces, ionic interactions, and hydrophobic effects) among the active components.[15,16] Our previous study has demonstrated that GL can self-assemble into nanomicelles, significantly enhancing the intestinal absorption and bioavailability of Pae.[18] Glycyrrhiza protein (GP) has also been reported to self-assemble into functional nanoparticles that are capable of significantly increasing solubility, promoting absorption, and enhancing the bioactivity of drugs.[19–22] The self-assembled GP nanoparticles were also found to increase the intestinal absorption of Pae.[23]

However, the formation of self-assembled nanoparticles in SGD (SGD-SAN) is not achieved solely by GL or GP, but rather results from the synergistic interaction of multiple components. It remains unclear whether the nano-assemblies in SGD differ fundamentally from either GL self-assembled nanomicelles (GL-SNM) or GP self-assembled nanoparticles (GP-SAN).

Therefore, the present study was performed to systematically compare the in vitro and in vivo characteristics of three nano-assemblies of different components from SGD (SGD-SAN, GL-SNM, and GP-SAN), with particular emphasis on their differential effects on oral absorption of Pae. SGD-SAN was separated and then identified for its composition. GL-SNM and GP-SAN were self-assembled according to the main components obtained from the composition analysis of SGD-SAN and loaded with Pae, named Pae GL-SNM and Pae GP-SAN, respectively. The SGD-SAN, Pae GL-SNM, and Pae GP-SAN were characterized in terms of particle size, zeta potential, morphology, drug loading, and in vitro release behavior. The single-pass intestinal perfusion and pharmacokinetic studies of SGD-SAN, Pae GL-SNM, and Pae GP-SAN following oral administration were performed to evaluate their absorption-enhancing effect. These comprehensive comparisons will elucidate the structure-function relationships underlying SGD's enhancement of Pae absorption, which is critical for revealing the synergistic mechanisms of multi-component interactions in TCM and clarifying the scientific basis of TCM compatibility. Moreover, clarifying these nano-assemblies' contributions may guide the development of novel TCM-based drug delivery systems and more effective TCM-derived formulations, providing support for the modern application of TCM.

Materials and Methods

Materials

PRA and GRR were purchased from Jiangxi Peng's Gaoyaotang Sliced Herb Co., Ltd. The herbal materials were authenticated by the Chief Pharmacist Ping Ying from the Department of Pharmacy, Jiangxi Provincial People's Hospital (the First Affiliated Hospital of Nanchang Medical College), PR China. Pae (purity > 95%), GL (purity > 95%), Pae reference standard (purity > 98%), and puerarin (internal standard, purity > 98%) were obtained from Baoji Herbest Bio-Tech Co., Ltd (Xian, PR China). HPLC-grade methanol and acetonitrile were purchased from Sigma-Aldrich (USA). 3500 Da dialysis bag was obtained from Shanghai Yuanye Biotechnology Co., Ltd. (Shanghai, China). All other chemicals used were of analytical grade.

Animals

Male Sprague-Dawley rats (weight 180–200 g, 6 weeks old) were obtained from SPF (Beijing) Biotechnology Co., Ltd. (Beijing, China). All rats were housed in an environmentally controlled breeding room (25 ± 2 °C, 60% humidity, and 12 h cycle of light and dark) and received ad libitum access to water and food. All animal experiments were conducted in compliance with the NIH Guidelines for the Care and Use of Laboratory Animals and were approved by the Institutional Ethics Committee of Nanchang Medical College (No. NYLLSC20240408).

Separation and Composition Analysis of SGD-SAN

Separation of SGD-SAN

SGD-SAN was separated as follows:[24] PRA and GRR herbs were weighed at a ratio of 1:1 (25 g + 25 g) and soaked in deionized water (500 mL) for 30 min. The mixture was boiled twice with 10- and 8-fold volumes (v/w) of deionized water (500 mL and 400 mL per 50 g herbs), each for 1 h. After filtration through eight layers of gauze, the two decoction liquids were combined and concentrated to 1 g/mL (crude drug equivalent) by rotary evaporation at 50 °C under reduced pressure (−0.08 MPa). After SGD preparation, SGD-SAN was obtained using a combined centrifugation-dialysis approach. SGD (50 mL) was centrifuged at 4000 rpm for 30 min to remove the precipitates. The supernatant (5 mL) was dialyzed against 200 mL of deionized water for 30 min using a 3500 Da molecular weight cutoff (MWCO) dialysis bag (25 mm flat width) at room temperature with constant agitation at 200 rpm, and then the liquids in dialysis bag was centrifuged at 13000 rpm for 30 min to remove the precipitates. The dialysis and

centrifugation operations were repeated twice. Through the above operations, the liquid inside the dialysis bag was freeze-dried and collected as SGD-SAN.

Composition Analysis of SGD-SAN

The composition of SGD-SAN was analyzed using a BCA assay kit, phenol-sulfuric acid method, and high-performance liquid chromatography (HPLC). The protein content of SGD-SAN was determined using a BCA assay kit according to the manufacturer's instructions. The polysaccharide content of the SGD-SAN was measured by the phenol-sulfuric acid method.[25] About of 20 mg SGD-SAN was dispersed in 10 mL of methanol, followed by ultrasonication for 10 min. After centrifugation at 8000 rpm for 10 min, the supernatant was filtered through 50 nm filters (Sigma-Aldrich, St Louis, MO, USA) for quantitative analysis of the main components by HPLC using an LC-20AD HPLC system (Shimadzu, Tokyo, Japan). Chromatographic separation was performed on an Inertsil® ODS-3 column (250 mm × 4.6 mm, 5 μm, Shimadzu, Tokyo, Japan) using a mobile phase of acetonitrile and 0.1% phosphoric acid solution with gradient elution (Table 1). The flow rate was maintained at 1.0 mL/min, with the column temperature set at 30 °C. Detection was performed at a wavelength of 237 nm and the injection volume was 10 μL.

Extraction of GP and Preparation of Pae GP-SAN

GP extraction from GRP was performed by the acetone precipitation method[22] with some modifications. Briefly, GRP decoction pieces were mixed with deionized water at ratio of 1:5 (w/v) and extracted under ultrasonication for 30 min at 60 °C. The resulting mixture was filtered through a double-layer filter cloth and centrifuged at 4,000 rpm for 15 min to remove residues. The supernatant was precipitated with 1.5 times volume of acetone, incubated at −20 °C for 30 min. The precipitates were collected by centrifugation at 4,000 rpm for 15 min and then freeze-dried to yield GP. The obtained GP was determined by sodium dodecyl sulfate−polyacrylamide gel electrophoresis (SDS-PAGE). The proteins were mixed with loading buffer and then heated at 95 °C for 10 min for protein denaturation. The denatured protein samples were separated by SDS-PAGE at 80 V to 120 V, and the protein bands were stained with Coomassie Brilliant Blue and compared with the protein standard.

The Pae GP-SAN was prepared by an ultrasonic dispersion method. Briefly, 16 mg of GP and 12 mg of Pae were added to 4 mL of deionized water and sonicated (JK-50B, Hefei Jinnick Medical Technology Co., Ltd., Hefei, China) at 250 W (50 Hz) for 25 min. After cooling to room temperature, the mixture was filtered through a 0.80 μm filter to obtain Pae GP-SAN.

Preparation of Pae GL-SNM

The Pae GL-SNM was fabricated via the film dispersion method, with a formulation consistent with that of our previous study.[18] Briefly, GL (40 mg) was dissolved in 10 mL of absolute ethanol in a 50 mL pear-shaped flask and then evaporated by rotary evaporator (RE-2000B, Shanghai Yarong Biochemistry Instrument Factory, Shanghai, China) at 50 °C to obtain a thin film of GL. The obtained film was hydrated with 9.2 mL of deionized water through ultrasonication in a 50 °C water bath to form a micellar suspension. Then, 10 mg of Pae was dissolved in 0.8 mL of ethanol and added

Table 1 Gradient Elution Conditions for Mobile Phase

Time (Min)	Acetonitrile (%)	0.1% Phosphoric Acid Solution (%)
0	10	90
10	20	80
18	21	79
19	23	77
35	40	60
40	50	50
50	50	50
53	10	90
60	10	90

dropwise to the micellar suspension at 50 °C under continuous magnetic stirring (MS-H280-Pro, Dragon Laboratory Instruments Ltd., Beijing, China) at 500 rpm. After cooling to room temperature, the resulting mixture was sonicated for 30 min in an ice-water bath using an ultrasonic cell disintegrator (JY92-IIN, Ningbo Scientz Biotechnology Co., Ltd., China) at 240 W with a 3 s pulse interval. The ethanol was removed by rotary evaporation, and the volume was adjusted to 10 mL with deionized water. Finally, Pae GL-SNM was obtained by filtration through 0.80 μm microporous membrane filters.

Characterization of Nano-Assemblies

Size Distribution and Zeta Potential Analysis

The particle size and polydispersity index (PDI) of SGD-SAN, Pae GP-SAN, and Pae GL-SNM were determined by dynamic light scattering (DLS) using a Zeta-sizer (Malvern Zetasizer Pro, Worcestershire, UK). Samples were appropriately diluted with deionized water, equilibrated at 25 °C for 2 min prior to measurement, and analyzed at 25 °C with a scattering angle of 173°. Zeta potential was estimated by determining the electrophoretic velocity of the particles using the same instrument.

Morphology Evaluation

The morphologies of SGD-SAN, Pae GP-SAN, and Pae GL-SNM were observed by transmission electron microscopy (TEM, Tecnai G2F20, FEI, Eindhoven, Netherlands). After appropriate dilution with deionized water, one drop of the sample was deposited onto a 200-mesh copper grid, blotted with filter paper, and dried at room temperature. Images were obtained by TEM at 80 kV for morphological evaluation.

Encapsulation Efficiency and Drug Loading

The drug encapsulation efficiency (EE) and drug loading (DL) of Pae GP-SAN and Pae GL-SNM were determined by ultrafiltration method.[18,26] Briefly, 0.4 mL of sample was placed into the upper chamber of ultrafiltration centrifugal tube tubes (3 kDa, Millipore Corporation, Billerica, MA, USA) and centrifuged at 8000 rpm for 10 min. The filtrate was diluted 10-fold with methanol and the free Pae concentration was quantified by HPLC (LC-20AD, Shimadzu, Tokyo, Japan). The chromatographic separation was carried out on Inertsil® ODS-3 column (250 mm × 4.6 mm, 5 μm, Shimadzu, Tokyo, Japan) with column temperature maintained at 40 °C and mobile phase of acetonitrile and 0.1% phosphoric acid (17: 83, v/v) at a flow rate of 1 mL/min. Detection was performed at 231 nm with an automated injection volume of 20 μL. The total Pae content in Pae GL-SNM or Pae GP-SAN was measured after extraction with 50-fold methanol in an ultrasonic bath. The EE and DL were calculated as follows:

$$EE(\%) = \frac{W_t - W_f}{W_t} \times 100\%$$

$$DL(\%) = \frac{W_t - W_f}{W_t - W_f + W_c} \times 100\%$$

where W_t is the total amount of Pae in Pae GP-SAN or Pae GL-SNM, W_f is the amount of free Pae unencapsulated in Pae GP-SAN or Pae GL-SNM, W_c is the total amount of GL or GP added. The drug loading (DL) of SGD-SAN was calculated by the Pae content in SGD-SAN, whereas the drug encapsulation efficiency (EE) was calculated as the ratio of the Pae content in SGD-SAN to the total Pae in SGD.

In vitro Drug Release

The Pae release from SGD-SAN, Pae GP-SAN, and Pae GL-SNM in vitro was investigated using a dialysis method and compared with that of Pae solution. The simulated gastric fluid (SGF, pH 1.2) and simulated intestinal fluid (SIF, pH 6.8) were selected as release media, respectively. All samples with dose equivalent to 10 mg Pae were placed into a dialysis bag (MWCO: 3500 Da; flat width: 25 mm, effective length: 30 mm). The bag was mounted with its symmetrical axis perpendicular to the direction of horizontal stirring to minimize boundary layer effects. Both ends were sealed with clips and immersed into 200 mL of release medium maintained at 37 ± 1 °C, and stirred at 100 rpm. At various time points

(0.25, 0.50, 0.75, 1, 2, 4, 6, 8, and 12 h), 1 mL aliquots were withdrawn and replaced with an equal volume of media. Each sample was filtered through a 50 nm filter, and the Pae concentration was determined by the same HPLC method as described in the determination of EE and DL. Drug release profiles were plotted as the cumulative % drug release versus time.

Single-Pass Intestinal Perfusion Study

The intestinal absorption of SGD-SAN, Pae GP-SAN, and Pae GL-SNM was investigated by in situ single-pass intestinal perfusion method[18,27,28] and compared with that of Pae solution. Male SD rats were fasted for 12h with free access to water before the perfusion experiment, and then were anesthetized by intraperitoneal injection of pentobarbital sodium (40 mg/kg). The anesthetized rats were fixed in a supine position on a homeothermic blanket to maintain normal body temperature, and a midline incision of the abdomen was made. Approximately 10 cm segment of either the jejunum or ileum was carefully cannulated on two ends with plastic tubing and ligated using silk sutures. The dissected intestinal segments were gently rinsed with 37 °C saline to clear the segment and then attached to a peristaltic pump (L100-1S-1/DG-2, Baoding Longer Precision Pump Co., Ltd., Baoding, China). The entire surgical area was covered with a piece of sterile absorbent gauze wetted with saline (37 ± 1°C). Initially, the intestinal segment was perfused with blank Krebs-Rings (K-R) solution at a flow rate of 0.2 mL/min for 30 min to remove any residue. Then, the K-R solution containing different Pae samples (SGD-SAN, Pae GL-SNM, Pae GP-SAN, and Pae solution) at the same Pae concentration of 20 μg/mL[29] were perfused at a flow rate of 0.2 mL/min for 30 min to ensure steady-state conditions, and the outlet perfused samples were collected in pre-weighed vials at 15 min intervals up to 90 min and then weighed. The perfusion rate of 0.2 mL/min is designed to simulate the physiological state, reduce intestinal injury, and is physiologically equivalent to the 2.0–3.0 mL/min rate used in human jejunal perfusion.[30–32] The collected samples were stored at −20 °C until analysis by the same HPLC method as described in determination of EE and DL. Finally, the animals were euthanized with an overdose of isoflurane, and the length and inner diameter of the intestinal segment were measured. The gravimetric method was used to determine net water flux (water absorption and efflux in the intestinal segment).[27–29] The absorption rate constant (K_a) and effective permeability coefficient (P_{eff}) of Pae in intestinal segments were calculated using the following equations:

$$K_a = \left(1 - \frac{C_{out}V_{out}}{C_{in}V_{in}}\right)\frac{Q}{\pi r^2 l}$$

$$P_{eff} = \frac{-Q\ln\left(\frac{C_{out}V_{out}}{C_{in}V_{in}}\right)}{2\pi r l}$$

where C_{in} and C_{out} are the concentrations of the test drug in the effluent perfusate through the inlet and outlet tubes (μg/mL), respectively. V_{in} and V_{out} represent the inlet and outlet volumes of the effluent perfusate (mL), respectively. Q is the perfusion volume flow rate (mL/h). r and l are the radius and the length of the perfused intestinal segment, respectively.

Pharmacokinetics Study

All rats were acclimated for one week and fasted for 12 h before the experiments. Twenty-four rats were randomly divided into four groups of six animals per group and received Pae solution, SGD-SAN, Pae GL-SNM, and Pae GP-SAN via gavage at a dose of 100 mg/kg Pae.[18] After administration, approximately 0.5 mL of whole blood was collected from the orbital venous plexus at 0.083, 0.167, 0.25, 0.5, 0.75, 1, 2, 4, 6, 8, 12 and 24 h, and then placed into heparinized tubes. The plasma samples were obtained by centrifugation at 5000 rpm for 10 min, and stored at −80 °C until analysis.

The plasma samples were processed according to our previous study,[18] and the Pae concentrations in plasma was determined by a validated HPLC/MS/MS system with puerarin as an internal standard (IS). An LC-30AD HPLC system (Shimadzu, Tokyo, Japan) was used for chromatographic separation with a Shim-pack Scepter C18 column (2.1 × 100 mm, 3 μm particle size, Shimadzu, Tokyo, Japan) maintained at 40 °C. The mobile phases consisted of 0.1% aqueous formic acid (A) and methanol (B) with gradient washing as follows: 0 ~ 1.1 min, 5%B; 1.1 ~ 2.4 min, 5 ~ 95% B; 2.4 ~ 4.0 min, 95%B; 4.0 ~ 4.5 min, 95 ~ 5%B; 4.5 ~ 6.0 min, 5%B. The flow rate was 0.3 mL/min and the injection

volume was 5 μL. A TRIPLE QUAD™ 4500MD mass spectrometer (AB SCIEX, Massachusetts, USA) was interfaced via electrospray ionization (ESI) source operating in positive ion mode at 550°C. The nebulizer gas (Gas 1), heater gas (Gas 2), curtain gas (CUR), and collision activated dissociation gas (CAD) were set to 55, 55, 33, and 8 instrument units, respectively. The quantification of Pae and Pue (IS) were quantified in the MRM mode using the pseudo-molecular (Q1) to fragment (Q3) ion transitions and the optimal declustering potential (DP), collision energy (CE), collision cell exit potential (CXP), and entrance potential (EP), as shown in the following conditions (Table 2).

Determination of Dominant Driving Forces in Self-Assemblies

To elucidate the dominant driving forces for the formation of SGD-SAN, Pae GP-SAN, and Pae GL-SNM, chemical interference agents (NaCl, urea, and Tween 20) were added, coupled with particle size detection, to identify the types of intermolecular forces in the self-assemblies.[20,33,34]

Statistical Analysis

The main pharmacokinetic parameters were calculated by DAS 2.0. All the experimental data were expressed as the mean ± standard deviation (mean ± SD). The SPSS 21.0 software was used to analyze the statistical data. First, the normality test and homogeneity of variance test of the data were performed. If the data meet the assumptions of normal distribution and homogeneity of variance, one-way analysis of variance (ANOVA) followed by the least significant difference post-hoc test was used to compare the differences among these groups. Otherwise, it was determined by Games–Howell test (heterogeneous variance) or Mann–Whitney *U*-test (non-normal distribution). Probability values $P < 0.05$ meant the difference was statistically significant.

Results and Discussions

Separation and Composition Analysis of SGD-SAN

According to our separation method, the average yield of SGD-SAN is (12.93 ± 0.58) %. Nine active ingredients were determined by HPLC. As shown in Figure 1A, the contents of isoliquiritin, liquiritigenin, benzoylpaeoniforin, and isoliquiritigenin were less than 0.2%, the contents of alibiflorin, liquiritin apioside, and liquiritin were about 1.25%, 0.97%, and 1.18%, while the contents of Pae and GL were 4.54% and 4.32%, respectively. These results suggested that Pae and GL were the main active ingredients. The protein content of SGD-SAN determined by BCA kit was about 61.91% (Figure 1B), accounting for most of the weight of SGD-SAN. In addition, the polysaccharide content of SGD-SAN was about 37.58%, while total content of 9 kinds of active ingredients was 12.69% (Figure 1B). The total content of all ingredients exceeded 100% (112.18%), which may be attributed to the overestimation of protein quantification owing to the presence of glucose[35] and repeated measurement of part carbohydrate components due to the presence of glycosides.

Preparation of Pae GP-SAN and Pae GL-SNM

To clarify the effects of nano-assemblies in SGD on Pae bioavailability, two new nanoformulations were prepared based on the chemical composition of SGD-SAN and their self-assembly properties. In our previous study, nanoparticles were mainly observed in single decoction of GRR and co-decoction of GRR and PRA, but only few nanoparticles were formed in single decoction of PRA[24] We speculated that nano-assemblies in SGD were mainly formed from the GRR components. The protein accounting for most of the weight of SGD-SAN was found to mainly come from GRR,[36] and can self-assemble into nanostructures with functional capability to encapsulate active ingredients.[19–22] Therefore, GP was extracted by an acetone precipitation method[22] with a modification and was exploited to fabricate Pae GP-SAN. The extracted GP was characterized by SDS-PAGE, and the band of GP was located between 25–35 kDa (Figure 1C). In addition, GL was the main active ingredient and has been reported to form nanomicelles by self-assembly to improve the

Table 2 Mass Spectrometry Conditions

Chemical Substance	Q1 (Da)	Q3 (Da)	DP (v)	CE (v)	CXP (v)	EP (v)
Pae	498.0	179.0	44	26	20	10
Pue (IS)	417.2	297.1	80	37	21	10

https://doi.org/10.2147/IJN.S544429

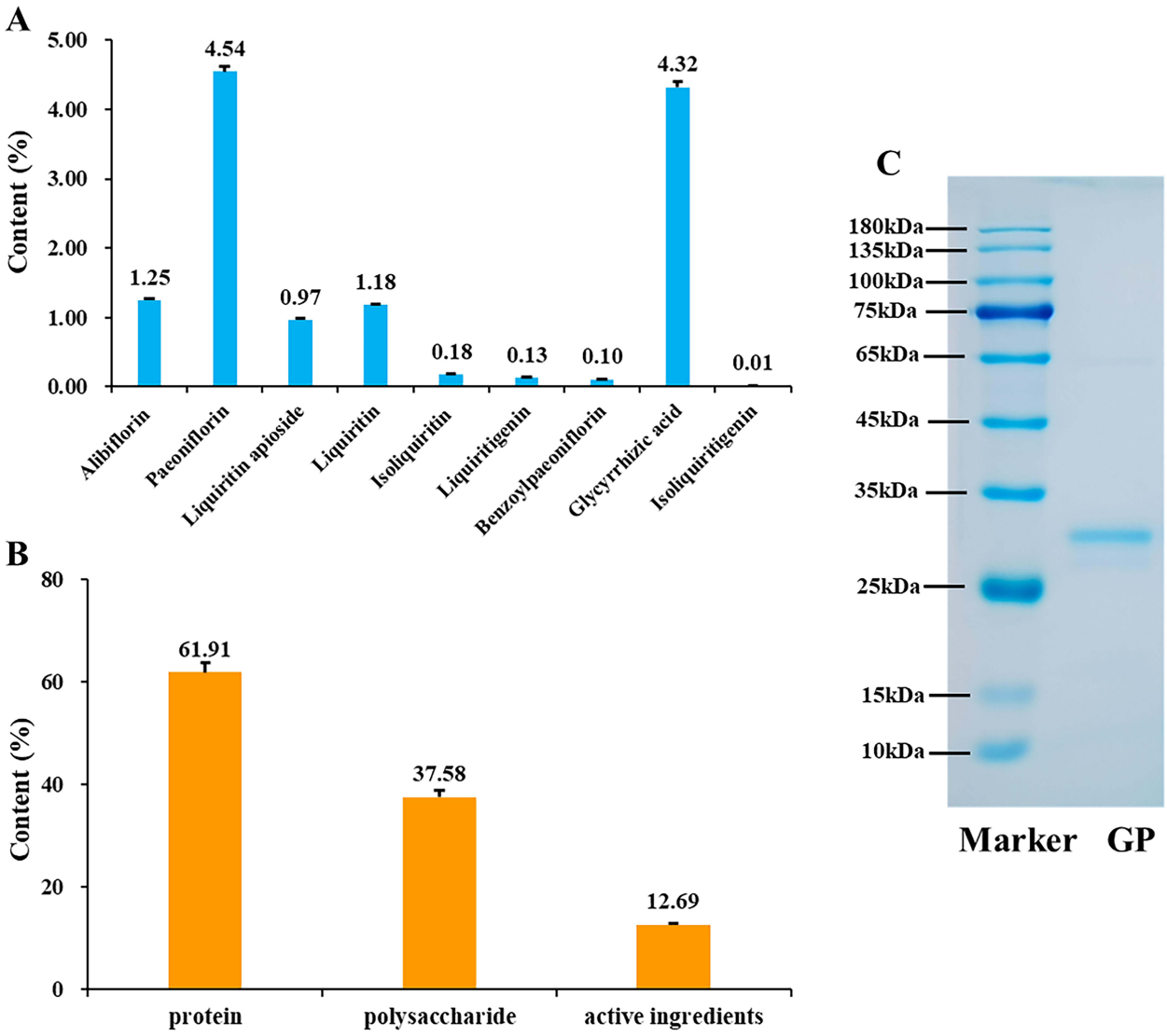

Figure 1 Composition analysis of SGD-SAN. **(A)**. Composition of SGD-SAN with standard substances by HPLC (Data are presented mean ± SD.). **(B)**. Proportion of proteins, polysaccharide, and active ingredients in SGD-SAN (Data are presented mean ± SD.). **(C)**. SDS-PAGE bands of GP.

oral absorption of natural molecules and therapeutic agents.[18,37–39] Therefore, Pae GL-SNM was fabricated via the film dispersion method, with a formulation consistent with that of our previous study.[18]

Characterization of Nano-Assemblies

The physicochemical properties of the three nano-assemblies are presented in Table 3 and Figure 2. Significant differences were observed in the physicochemical properties of the three nano-assemblies. The mean particle sizes of SGD-SAN, Pae GL-SNM, and Pae GP-SAN were around 130, 150 and 180 nm (Figure 2 A1-A3), respectively, and their PDI were 0.354, 0.167, and 0.154, respectively. The PDI value exceeding 0.3 for SGD-SAN reflects a broad particle size

Table 3 Physicochemical Properties of Nano-Assemblies (Mean ± SD, n=3)

	SGD-SAN	Pae GL-SNM	Pae GP-SAN
Zeta potential (mV)	−14.75 ± 1.26	−35.88 ± 1.80	−14.76 ± 1.24
EE (%)	44.07 ± 3.29	47.94 ± 1.17	36.56 ± 0.95
DL (%)	5.54 ± 0.47	10.70 ± 0.23	21.52 ± 0.44

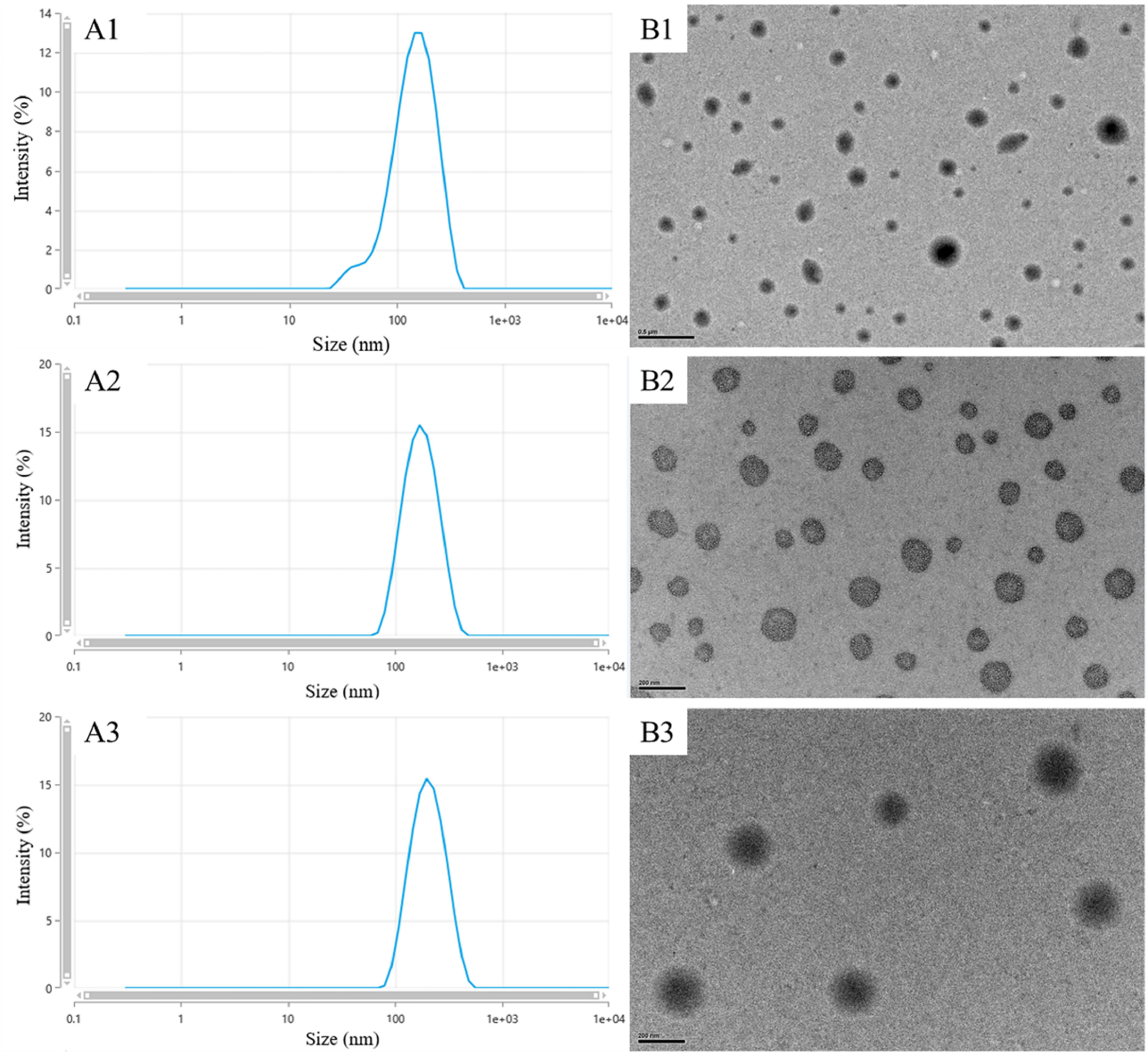

Figure 2 Particle size distribution and SEM images of Pae nano-formulations. (A1) and (B1) representing particle size distribution (PS:133 ± 13 nm, PDI:0.354 ± 0.015) and SEM images of SGD-SAN; (A2) and (B2) are particle size distribution (PS:154 ± 8 nm, PDI:0.167 ± 0.013) and SEM images of Pae GL-SNM; (A3) and (B3) are particle size distribution (PS:184 ± 7 nm, PDI:0.154 ± 0.009) and SEM images of Pae GP-SAN.

distribution, whereas both Pae GL-SNM and Pae GP-SAN exhibited PDI values below 0.2, suggesting a narrow size distribution.[40] SGD-SAN exhibited the minimum particle size and maximum PDI, which may be due to its complex composition and sources. Repeated dialysis and centrifugation effectively removed larger particles, resulting in reduced particle size. The complex composition of SGD-SAN may contribute to its instability, leading to a broad particle size distribution. The TEM images demonstrated that SGD-SAN, Pae GL-SNM, and Pae GP-SAN were spherical in shape (Figure 2 B1-B3), with estimated average sizes of 50–300 nm for SGD-SAN and 100–200 nm for Pae GL-SNM and Pae GP-SAN, which is similar with the DLS measurements.

Both SGD-SAN and Pae GP-SAN exhibited zeta potentials of approximately −15 mV, suggesting limited colloidal stability, whereas Pae GL-SNM demonstrated a substantially higher absolute zeta potential (−35.88 mV), which was associated with enhanced stability due to stronger electrostatic repulsion.[18] The similar zeta potentials observed for SGD-SAN and Pae GP-SAN may be attributed to their shared protein constituents, which likely dominate the surface charge characteristics of these nanoparticles. The EE of SGD-SAN, Pae GL-SNM, and Pae GP-SAN were 44.07%, 47.94% and

https://doi.org/10.2147/IJN.S544429

36.56%, respectively. The relatively low EE (less than 50%) observed for SGD-SAN, Pae GL-SNM, and Pae GP-SAN could be attributed to the high hydrophilicity of Pae.[41] The DL of SGD-SAN, Pae GL-SNM and Pae GP-SAN were 5.54%, 10.70%, and 21.52%, respectively. The discrepancies in DL among SGD-SAN, Pae GL-SNM, and Pae GP-SAN are likely due to differences in the structural composition and size of the nanoparticles. SGD-SAN exhibited the lowest DL of Pae, because it encapsulated not only Pae but also other active ingredients, such as albiflorin, benzoylpaeoniflorin, and liquiritin.

In Vitro Drug Release

The in vitro release profiles of SGD-SAN, Pae GL-SNM, and Pae GP-SAN are shown in Figure 3. Similar drug release profiles were observed for the same Pae formulations in both the SGF and SIF. Compared to the Pae solution, Pae release from the three nano-assemblies (SGD-SAN, Pae GL-SNM, and Pae GP-SAN) exhibited significantly slower kinetic profiles. About 100% of Pae was rapidly released from the Pae solution within 2 h, whereas only 50%-75% of Pae was released from SGD-SAN, Pae GL-SNM, and Pae GP-SAN in SGF and SIF, which is likely due to the sustained diffusion barrier imposed by the nano-assemblies matrix and drug-carrier interactions.[42] In addition, the Pae release from three nano-assemblies within 6 h in SGF followed the order: Pae GP-SAN > SGD-SAN > Pae GL-SNM, with Pae GP-SAN exhibiting the fastest release kinetics (74.61% at 2 h vs 61.54% for SGD-SAN and 53.20% for Pae GP-SAN), likely due to protein hydrolysis of GP in an acidic environment, which compromises the structural integrity of nano-assemblies and promotes payload liberation. Pae GL-SNM exhibited a relatively lower cumulative Pae release (53.20%) in SGF than in SIF (64.11%), which may be due to the suppression of Pae GL-SNM disassembly under low pH conditions, thereby maintaining the structural integrity of micelles and delaying drug release. The sustained release of Pae from the nano-assemblies may be beneficial for the oral absorption of Pae by facilitating prolonged mucosal interactions.[43]

Intestinal Absorption Characteristics of Nano-Assemblies

The intestinal perfusion studies in rats are the most reliable and cost-effective option among all methods for assessing intestinal drug absorption due to the high correlation between human and rat small intestinal permeability (r^2 = 0.8–0.95).[29,44] The in situ intestinal perfusion has been widely used to study the absorption of drugs in the intestine.[18,28,29,39,45] Therefore, the absorptive behaviors of SGD-SAN, Pae GL-SNM, Pae GP-SAN, and Pae solution were compared by the in situ intestinal perfusion method, and gravimetry was employed instead of the classic phenol red method to determine perfusate volume changes in our study, owing to the partial intestinal absorption of phenol red.[29]

The K_a and P_{eff} obtained from the single-pass intestinal perfusion models are shown in Figure 4. Pae solution showed similar K_a and P_{eff} values in the jejunum and ileum. The K_a and P_{eff} values of SGD-SAN, Pae GL-SNM and Pae GP-SAN were higher than those of the Pae solution, indicating increased intestinal absorption of Pae by nano-assemblies. This may be explained as follows: firstly, GL in SGD-SAN and Pae GL-SNM may reduce drug efflux through the inhibition of P-gp and increase drug penetration through the intestinal epithelium by increasing permeability and decreasing the elasticity modulus of the cell membranes.[46,47] Secondly, the excellent mucoadhesion of nanoparticles to GI prolongs the drug residence time, possibly leading to increased drug absorption.[48] Finally, internalization of nanoparticles by epithelial cells may also contribute to intestinal absorption of Pae.[49] Among the three nano-assemblies, Pae GP-SAN showed the highest K_a and P_{eff} values in the ileum, suggesting the best intestinal absorption. The possible explanation is as follows: a key distinction between the jejunum and the ileum lies in the presence of specialized structures such as Peyer's patches (PPs) in the latter.[50] The follicular-associated epithelial cells (FAE) are enriched in the PPs, where many membranous/microfold cells (M cells) reside in the FAE region.[51] M cells are specialized antigen-transporting cells characterized by abundant vesicles, short microvilli, and low enzymatic activity, with a primary function of transporting antigens from the intestinal lumen to the subepithelial lymphoid tissue.[52] Involved in antigen sampling, M cells have been extensively reported to possess strong transcytosis capacities to transport a wide range of particulate substances, including antigens, bacteria, viruses, and therapeutic nanoparticles. As an exogenous protein nanoparticle, Pae GP-SAN, with protein-rich composition, is likely to be recognized as antigenic substance and preferentially internalized by M cells, which likely accounts for its greater absorption in the ileum.[49]

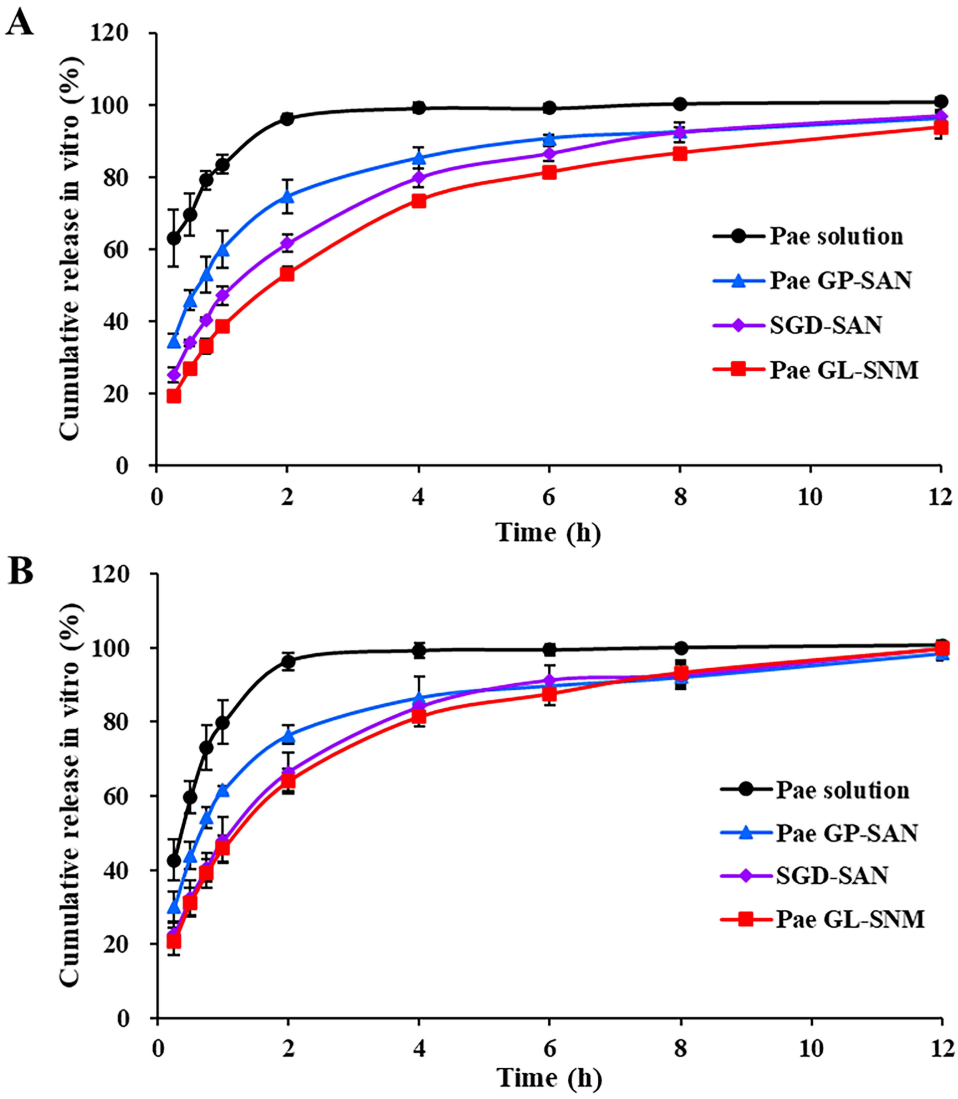

Figure 3 In vitro release profiles of Pae from Pae solution, SGD-SAN, Pae GL-SNM and Pae GP-SAN in SGF (**A**) and SIF (**B**) (mean ± SD, n=3).

Pharmacokinetics of Nano-Assemblies

The plasma concentration-time curves of Pae after oral administration of Pae solution, SGD-SAN, Pae GL-SNM, and Pae GP-SAN are shown in Figure 5, and the main pharmacokinetic parameters are presented in Table 4. In agreement with our previous findings,[18] Pae solution demonstrated poor oral absorption, as evidenced by its low C_{max} (964.89 ± 128.81 ng/mL) and AUC_{0-t} (5676.14 ± 311.61 ng/mL·h), which could be attributed to its high hydrophilicity, P-gp mediated efflux, and hydrolysis in the intestine.[53] Compared with the Pae solution, SGD-SAN exhibited a relatively higher plasma concentration of Pae at all time points following oral administration. The C_{max} (1907.48 ± 245.22 ng/mL) and AUC_{0-t} (8241.69 ± 944.62 ng/mL·h) of Pae after oral administration of SGD-SAN were significantly higher than those of Pae solution, indicating significant enhancement in the oral bioavailability of Pae. Furthermore, the results also suggested that the bioavailability improvement of Pae by oral administration of SGD may be related to the formation of SGD-SAN during decoction. The bioavailability improvement of Pae by SGD-SAN can be attributed to the prolonged drug release and the increased intestinal absorption. In addition, both the bioadhesive properties and the overall transmembrane capacity of nanoparticles also probably contribute to the enhanced Pae absorption.[42,54]

Notably, the bioavailability of Pae was also significantly improved by the oral administration of Pae GL-SNM and Pae GP-SAN, as evidenced by the higher AUC_{0-t} (9362.52 ± 854.15 ng/mL·h for Pae GL-SNM and 11209.01 ± 2093.72

https://doi.org/10.2147/IJN.S544429

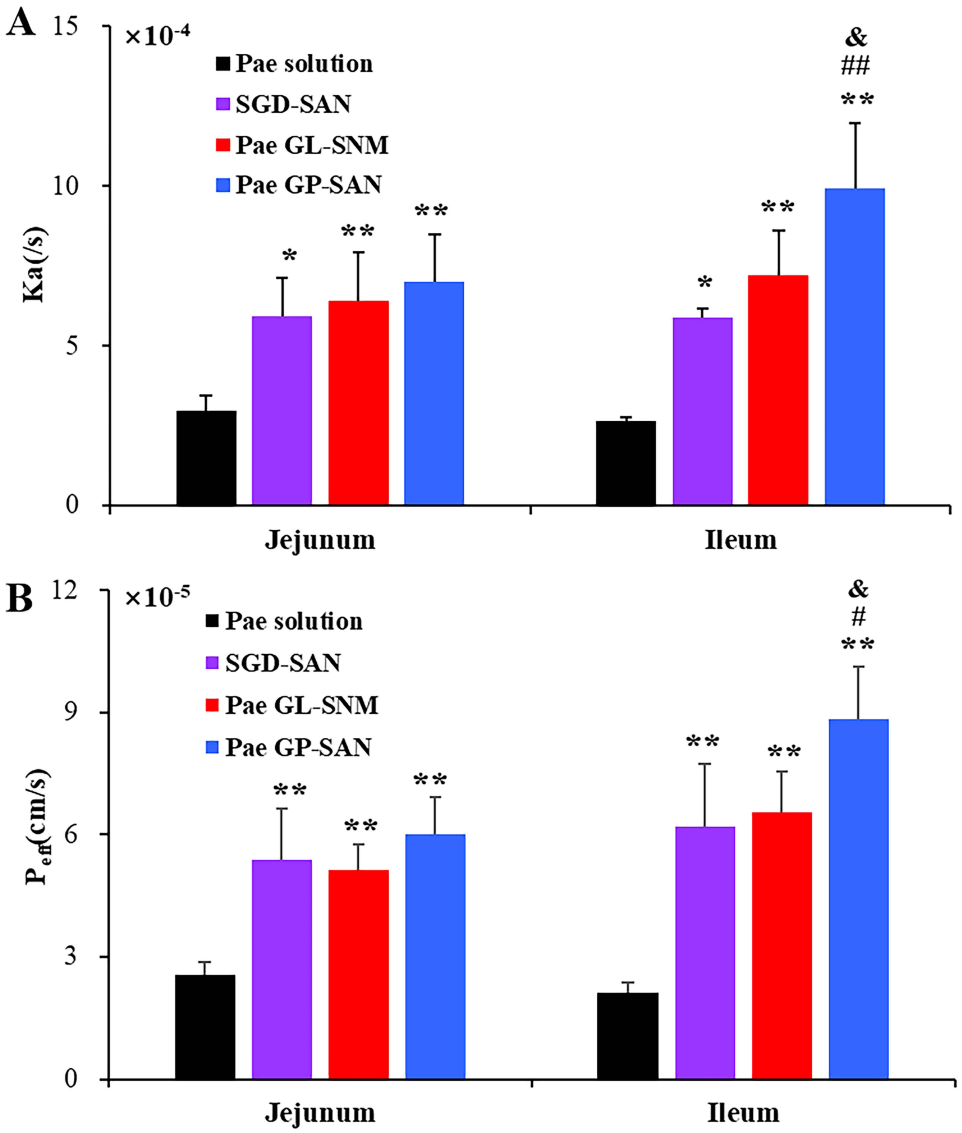

Figure 4 The K_a (**A**) and P_{eff} (**B**) of Pae from Pae solution, SGD-SAN, Pae GL-SNM and Pae GP-SAN in the jejunum and ileum (mean ± SD, n=3; *P < 0.05, **P < 0.01 vs Pae solution; $^{\#}P$ < 0.05, $^{\#\#}P$ < 0.01 vs SGD-SAN; $^{\&}P$ < 0.05 vs Pae GL-SNM).

ng/mL·h for Pae GP-SAN). The same reason as proposed above with SGD-SAN can be employed to interpret the bioavailability improvement of Pae by the oral administration of Pae GL-SNM and Pae GP-SAN. Moreover, Pae GP-SAN showed significantly higher $AUC_{0\text{-}t}$ as compared to SGD-SAN, which could be explained by the increased intestinal absorption in the ileum. Both intestinal perfusion and pharmacokinetic studies demonstrated that SGD-SAN, Pae GL-SNM, and Pae GP-SAN significantly enhanced the oral absorption of Pae, with Pae GP-SAN exhibiting the best oral absorption. These results suggested that nano-assemblies, particularly protein-based GP-SAN, overcome the absorption barriers of Pae through ileum-targeted uptake, sustained release, and nanoparticle bioadhesion, providing a structural foundation for SGD's bioavailability-enhancing effect.

Potential Formation Mechanisms of Nano-Assemblies

As is well known, urea and Tween 20 are capable of disrupting hydrogen bonds and hydrophobic interactions, respectively, while NaCl can reduce electrostatic interactions;[20] these chemical interference agents have been widely used to study the mechanism of nanocomplex formation.[33,34] To gain more insights into which dominant driving forces are present, we investigated the particle size change of SGD-SAN, Pae GP-SAN, and Pae GL-SNM after adding urea,

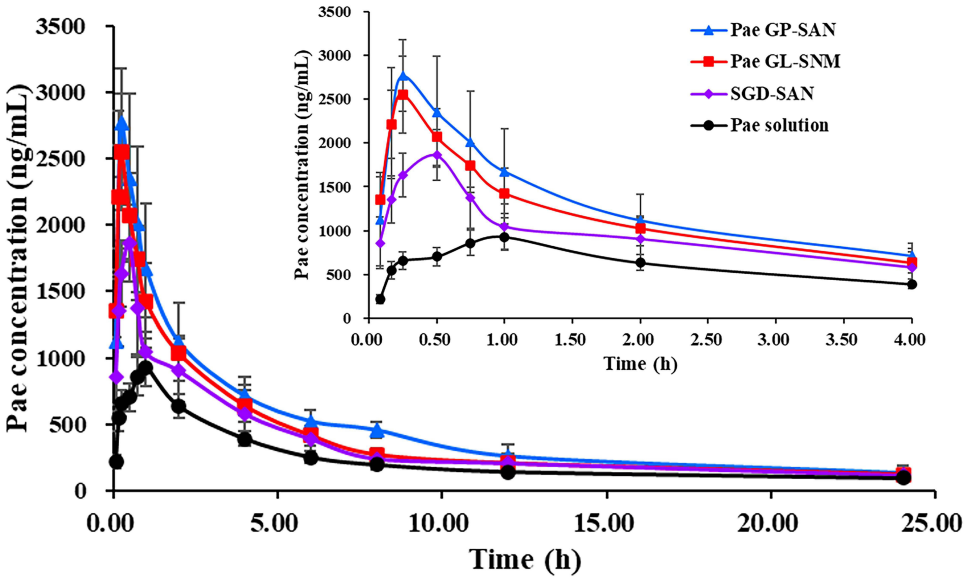

Figure 5 Plasma concentration-time curves of Pae following oral administration of Pae solution, SGD-SAN, Pae GL-SNM and Pae GP-SAN (mean ± SD, n=6).

NaCl, and Tween 20. As shown in Figure 6A, increasing concentrations of urea significantly increased the particle size of Pae GL-SNM, while exerting no effect on that of SGD-SAN and Pae GP-SAN, indicating that hydrogen bonds may not play a dominant role in driving the assembly or maintaining the structural stability of SGD-SAN and Pae GP-SAN, but play a non-negligible role in either the formation or, more notably, the structural stability of Pae GL-SNM.

Figure 6B showed that increasing concentrations of NaCl exerted no effect on the particle size of SGD-SAN, led to a slight increase in the particle size of Pae GP-SAN, and caused a significant increase in the particle size of Pae GL-SNM. Notably, when the NaCl concentration was equal to or higher than 0.05 M, Pae GL-SNM underwent obvious gelation. The absence of particle size change of SGD-SAN with increasing NaCl concentrations indicates that its stable dispersion is completely independent of electrostatic interactions. The slight particle size enlargement of Pae GP-SAN implies a weak reliance on electrostatic interactions. The significant particle size increase and subsequent gelation (at NaCl ≥ 0.05 M) of Pae GL-SNM demonstrate its strong dependence on electrostatic interactions.

Increasing concentrations of Tween 20 exerted a significant impact on the particle sizes of SGD-SAN, Pae GP-SAN, and Pae GL-SNM, but with distinct concentration-dependent trends (Figure 6C). The particle size increased significantly with rising Tween 20 concentration and tended to plateau (~800 nm) after the concentration reached 5 mM, while the particle size of Pae GP-SAN remained unchanged initially and then increased significantly (~1600 nm) when the Tween 20 concentration reached 10 mM. The results indicated that hydrophobic interactions play a critical role in maintaining the stability of SGD-SAN and Pae GP-SAN. For Pae GL-SNM, the particle size increased slightly to approximately 200 nm at Tween 20 concentrations below 2 mM, followed by a significant decrease to approximately 20 nm at and above 5 mM. This is because at low concentrations, Tween 20 only partially inserts into the Pae GL-SNM, causing a slight size increase due to structural loosening or shell expansion. However, once a critical concentration is exceeded, it sufficiently disrupts the hydrophobic interactions to disassemble the original micelles and form smaller mixed or Tween 20-dominated micelles, resulting in a significant size reduction.

Table 4 The Pharmacokinetic Parameters of Pae Following Oral Administration of Pae Solution, SGD-SAN, Pae GL-SNM and Pae GP-SAN (Mean ± SD, n=6)

Parameters	Pae Solution	SGD-SAN	Pae GL-SNM	Pae GP-SAN
AUC_{0-t} (ng/mL·h)	5676.14±311.61	8241.69±944.62**	9362.52±854.15**	11,209.01±2093.72**#
C_{max} (ng/mL)	964.89±128.81	1907.48±245.22**	2655.97±360.11**##	2896.04±255.01**##
T_{max} (h)	0.95±0.11	0.40±0.14**	0.23 ±0.04**#	0.28±0.13**
$T_{1/2z}$ (h)	10.25±4.50	9.70 ± 3.93	8.74± 4.66	9.50 ± 4.25
MRT_{0-t} (h)	7.19 ±0.40	6.70 ± 0.71	6.17 ± 0.19**	6.35 ± 0.28**

Note: **P < 0.01 vs Pae solution; #P < 0.05, ##P < 0.01 vs SGD-SAN.

https://doi.org/10.2147/IJN.S544429

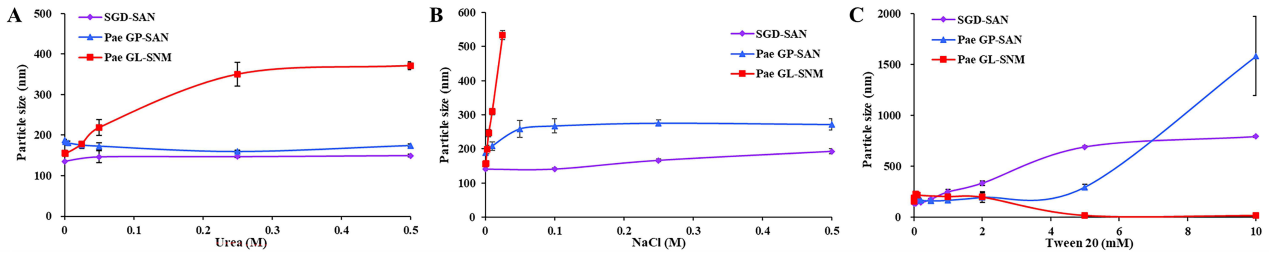

Figure 6 The particle size change of SGD-SAN, Pae GP-SAN, and Pae GL-SNM after adding urea (**A**), NaCl (**B**), and Tween 20 (**C**).

Based on the above results, we can draw the following conclusions: hydrophobic interactions serve as the common core force across all nano-assemblies, while their dependencies on other intermolecular forces differ significantly. Specifically, hydrophobic interactions act as the core driving force for the formation of Pae GL-SNM, with hydrogen bonds and electrostatic interactions jointly assisting in maintaining the structural stability of the formed micelles; for Pae GP-SAN, its formation is driven by a synergistic effect dominated by hydrophobic interactions and supplemented by electrostatic interactions; while for SGD-SAN, hydrophobic interactions may alone constitute the core force supporting its structural stability.

Conclusions

In this study, three nano-assemblies of different components from SGD (SGD-SAN, Pae GL-SNM, and Pae GP-SAN) were compared in vitro and in vivo, with particular emphasis on their differential effects on Pae bioavailability. Three nano-assemblies showed similar spherical shape, but exhibited significant differences in particle size (133 nm for SGD-SAN, 154 nm for Pae GL-SNM, and 184 nm for Pae GP-SAN), PDI, zeta potential, EE, and DL (5.54% for SGD-SAN, 10.70% for Pae GL-SNM, and 21.52% for Pae GP-SAN). While hydrophobic interactions act as the common core force driving the formation of all nano-assemblies, their dependencies on other intermolecular forces vary remarkably. SGD-SAN, Pae GL-SNM, and Pae GP-SAN exhibited sustained Pae release (50–75% over 12 h vs 100% for the Pae solution in 2 h). In situ intestinal perfusion experiments in rats showed significantly higher effective permeability coefficients (P_{eff}) for all nano-assemblies than the Pae solution, with Pae GP-SAN exhibiting the highest ileal absorption, which may be attributed to preferential M-cell uptake facilitated by its larger size and protein-rich composition. Pharmacokinetic studies further confirmed superior performance of Pae GP-SAN with the highest $AUC_{0\text{-}t}$ (11209.01 ± 2093.72 ng/mL·h) and C_{max} (2896.04 ± 255.01 ng/mL), representing 2.0-fold and 3.0-fold increases over Pae solution (5676.14 ± 311.61 ng/mL·h and 964.89 ± 128.81 ng/mL), respectively. Additionally, Pae GL-SNM and SGD-SAN significantly enhanced Pae bioavailability, with $AUC_{0\text{-}t}$ increased by 65% and 45%, respectively. These results suggested that nano-assemblies, particularly protein-based Pae GP-SAN, overcome the absorption barriers of Pae through ileum-targeted uptake, sustained release, and nanoparticle bioadhesion, thereby providing a structural basis for SGD's ability to enhance Pae bioavailability. The comprehensive comparisons elucidated the structure-function relationships underlying SGD-mediated improvements in Pae absorption. However, the reasons for the difference in Pae absorption among the three nano-assemblies remain unclear. In particular, no direct experimental evidence has been provided to support ileal M-cell uptake proposed as a key mechanism for Pae GP-SAN's superior absorption. Further studies should be performed to clarify their mechanisms for enhancing the oral absorption of Pae.

Acknowledgments

This work was partially supported by the National Natural Science Foundation of China (82260848), the Natural Science Foundation of Jiangxi Province (20232BAB216139), - the Technology Innovation Team of Jiangxi University of Traditional Chinese Medicine (CXTD22006)-, and the Innovation Special Fund for graduate students of Jiangxi University of Chinese Medicine (202510412257).

Author Contributions

All authors made a significant contribution to the work reported, whether that is in the conception, study design, execution, acquisition of data, analysis and interpretation, or in all these areas; took part in drafting, revising or critically

reviewing the article; gave final approval of the version to be published; have agreed on the journal to which the article has been submitted; and agree to be accountable for all aspects of the work.

Disclosure

The authors have no relevant financial or non-financial interests to disclose.

References

1. Wu Y, Li W, Zhang J, et al. Shaoyao-gancao decoction, a famous Chinese medicine formula, protects against APAP-induced liver injury by promoting autophagy/mitophagy. *Phytomedicine*. 2024;135:156053. doi:10.1016/j.phymed.2024.156053
2. Chang ZP, Deng GF, Shao YY, et al. Shaoyao-gancao decoction ameliorates the inflammation state in polycystic ovary syndrome rats via remodeling gut microbiota and suppressing the tlr4/nf-kappab pathway. *Front Pharmacol*. 2021;12:670054. doi:10.3389/fphar.2021.670054
3. Ding ZH, Wang N, Yang J, et al. Shaoyao gancao decoction in digestive system diseases: applications and mechanisms. *Zhongguo Zhong Yao Za Zhi*. 2024;23:6311–6319.
4. Lu J, Wang J, Yu L, et al. shaoyao-gancao decoction promoted microglia m2 polarization via the il-13-mediated jak2/stat6 pathway to alleviate cerebral ischemia-reperfusion injury. *Mediators Inflamm*. 2022;2022:1707122. doi:10.1155/2022/1707122
5. Zhou YX, Gong XH, Zhang H, et al. A review on the pharmacokinetics of paeoniflorin and its anti-inflammatory and immunomodulatory effects. *Biomed Pharmacother*. 2020;130:110505. doi:10.1016/j.biopha.2020.110505
6. Takeda S, Isono T, Wakui Y, et al. Absorption and excretion of paeoniflorin in rats. *J Pharm Pharmacol*. 1995;12A:1036–1040.
7. Chen LC, Chou MH, Lin MF, et al. Pharmacokinetics of paeoniflorin after oral administration of Shao-yao Gan-chao Tang in mice. *Jpn J Pharmacol*. 2002;3:250–255. doi:10.1254/jjp.88.250
8. Yoshida N, Koizumi M, Adachi I, et al. Inhibition of P-glycoprotein-mediated transport by terpenoids contained in herbal medicines and natural products. *Food Chem Toxicol*. 2006;12:2033–2039. doi:10.1016/j.fct.2006.07.003
9. Li X, Hu J, Wang B, et al. Inhibitory effects of herbal constituents on P-glycoprotein in vitro and in vivo: herb-drug interactions mediated via P-gp. *Toxicol Appl Pharmacol*. 2014;275(2):163–175. doi:10.1016/j.taap.2013.12.015
10. Hou YC, Lin SP, Chao PD. Liquorice reduced cyclosporine bioavailability by activating P-glycoprotein and CYP 3A. *Food Chem*. 2012;4:2307–2312. doi:10.1016/j.foodchem.2012.07.061
11. Xu CH, Wang P, Wang Y, et al. Pharmacokinetic comparisons of two different combinations of Shaoyao-Gancao Decoction in rats: competing mechanisms between paeoniflorin and glycyrrhetinic acid. *J Ethnopharmacol*. 2013;2:443–452. doi:10.1016/j.jep.2013.06.049
12. Sun H, Wang J, Lv J. Effects of glycyrrhizin on the pharmacokinetics of paeoniflorin in rats and its potential mechanism. *Pharm Biol*. 2019;1:550–554. doi:10.1080/13880209.2019.1651876
13. He R, Xu Y, Peng J, et al. The effects of 18β-glycyrrhetinic acid and glycyrrhizin on intestinal absorption of paeoniflorin using the everted rat gut sac model. *J Nat Med*. 2017;1:198–207. doi:10.1007/s11418-016-1049-2
14. Fang C, Wang Y, Pan Z. Formation of self-assembly aggregates in traditional Chinese medicine decoctions and their application in cancer treatments. *RSC Adv*. 2025;7:5476–5506. doi:10.1039/D4RA07212J
15. Dong YY, Guo Q, Gao Y, et al. Revealing the scientific connotation of compatibility of Chinese medicine medica based on self-assembly technology. *J Tradit Chin Med*. 2024;6:1288–1295.
16. Gao Y, Dong Y, Guo Q, et al. Study on supramolecules in traditional chinese medicine decoction. *Molecules*. 2022;10:3268.
17. Zhao Q, Luan X, Zheng M, et al. Synergistic mechanisms of constituents in herbal extracts during intestinal absorption: focus on natural occurring nanoparticles. *Pharmaceutics*. 2020;2:128. doi:10.3390/pharmaceutics12020128
18. Shen C, Shen B, Zhu J, et al. Glycyrrhizic acid-based self-assembled micelles for improving oral bioavailability of paeoniflorin. *Drug Dev Ind Pharm*. 2021;2:207–214. doi:10.1080/03639045.2020.1862178
19. Zhou J, Zhang J, Gao G, et al. Boiling licorice produces self-assembled protein nanoparticles: a novel source of bioactive nanomaterials. *J Agric Food Chem*. 2019;33:9354–9361.
20. Wang H, Song B, Zhou J, et al. Fabrication and characterization of curcumin-loaded nanoparticles using licorice protein isolate from Radix Glycyrrhizae. *Int J Biol Macromol*. 2024;255:128235. doi:10.1016/j.ijbiomac.2023.128235
21. Liu X, Ou X, Zhang T, et al. In situ neutrophil apoptosis and macrophage efferocytosis mediated by Glycyrrhiza protein nanoparticles for acute inflammation therapy. *J Control Release*. 2024;369:215–230. doi:10.1016/j.jconrel.2024.03.029
22. Li Y, Zhang D, Shi T, et al. De novo engineering of nanoformulation from traditional Chinese medicine mixtures for psoriasis. *Nano Res*. 2023;16 (4):5279–5291.
23. Dong YY. Study on the Absorption Mechanism of *Glycyrrhizin* Protein-Paeoniflorin Nanoparticles in Shaoyao Gancao Decoction. Master's Thesis, China Academy of Chinese Medical Sciences, 2024.
24. Shen CY, Zhu JJ, Dai B, et al. Effect of self-assembled nanoparticles from shaoyao gancao decoction on release and absorption of main components of baishao. *Zhongguo Zhong Yao Za Zhi*. 2021;9:2190–2196.
25. He YC, Shen BD, Shen CY, et al. Study on phase separation and anti-dermatophyte effect of Huangqin Decoction. *Zhong Cao Yao*. 2025;9:3099–3108.
26. Zhang K, Zhang Y, Li Z, et al. Essential oil-mediated glycerosomes increase transdermal paeoniflorin delivery: optimization, characterization, and evaluation in vitro and in vivo. *Int J Nanomed*. 2017;12:3521–3532. doi:10.2147/IJN.S135749
27. Sun W, Gao J, Fan R, et al. The effect of particle size on the absorption of cyclosporin a nanosuspensions. *Int J Nanomed*. 2022;17:1741–1755. doi:10.2147/IJN.S357541
28. Kuang G, Yi H, Zhu M, et al. Study of absorption characteristics of the total saponins from radix ilicis pubescentis in an In Situ Single-Pass Intestinal Perfusion (SPIP) Rat Model by Using Ultra Performance Liquid Chromatography (UPLC). *Molecules*. 2017;11:1867. doi:10.3390/molecules22111867

29. Yang XD, Wang C, Zhou P, et al. Absorption characteristic of paeoniflorin-6'-O-benzene sulfonate (CP-25) in in situ single-pass intestinal perfusion in rats. *Xenobiotica*. 2016;9:775–783. doi:10.3109/00498254.2015.1121553
30. Fagerholm U, Johansson M, Lennernäs H. Comparison between permeability coefficients in rat and human jejunum. *Pharm Res*. 1996;9:1336–1342. doi:10.1023/A:1016065715308
31. Lennernäs H. Human jejunal effective permeability and its correlation with preclinical drug absorption models. *J Pharm Pharmacol*. 1997;7:627–638. doi:10.1111/j.2042-7158.1997.tb06084.x
32. Reis JM, Dezani AB, Pereira TM, et al. Lamivudine permeability study: a comparison between PAMPA, ex vivo and in situ Single-Pass Intestinal Perfusion (SPIP) in rat jejunum. *Eur J Pharm Sci*. 2013;4-5:781–789. doi:10.1016/j.ejps.2012.12.025
33. Buecker S, Grossmann L, Loeffler M, et al. Thermal and acidic denaturation of phycocyanin from Arthrospira platensis: effects of complexation with λ-carrageenan on blue color stability. *Food Chem*. 2022;380:132157. doi:10.1016/j.foodchem.2022.132157
34. Chung JE, Tan S, Gao SJ, et al. Self-assembled micellar nanocomplexes comprising green tea catechin derivatives and protein drugs for cancer therapy. *Nat Nanotechnol*. 2014;11:907–912. doi:10.1038/nnano.2014.208
35. Zhao J, Zhao Q, Lu JZ, et al. Natural nano-drug delivery system in coptidis rhizoma extract with modified berberine hydrochloride pharmacokinetics. *Int J Nanomed*. 2021;16:6297–6311. doi:10.2147/IJN.S323685
36. Guo Q. Exploring the material basis of compatibility of Shaoyao-Gancao medicine pairs based on protein self-assembly. Master's Thesis, China Academy of Chinese Medical Sciences, 2022.
37. You G, Feng T, Zhang G, et al. Preparation, optimization, characterization and in vitro release of baicalein-solubilizing glycyrrhizic acid nano-micelles. *Int J Pharm*. 2021;601:120546. doi:10.1016/j.ijpharm.2021.120546
38. Tucker IM, Burley A, Petkova RE, et al. Adsorption and self-assembly properties of the plant based biosurfactant, Glycyrrhizic acid. *J Colloid Interface Sci*. 2021;598:444–454. doi:10.1016/j.jcis.2021.03.101
39. Yang FH, Zhang Q, Liang QY, et al. Bioavailability enhancement of paclitaxel via a novel oral drug delivery system: paclitaxel-loaded glycyrrhizic acid micelles. *Molecules*. 2015;3:4337–4356. doi:10.3390/molecules20034337
40. Wang F, Shen C, Chen F, et al. Quercetin nanocrystals stabilized by glycyrrhizic acid for liver targeted drug delivery: impact of glycyrrhizic acid concentrations. *Pharm Dev Technol*;2025. 1–10. doi:10.1080/10837450.2025.2591746
41. Cui Y, Mo Y, Zhang Q, et al. Microneedle-assisted percutaneous delivery of paeoniflorin-loaded ethosomes. *Molecules*. 2018;12:3371. doi:10.3390/molecules23123371
42. Kang JH, Jeong JH, Kwon YB, et al. Mucosal penetrative polymeric micelle formulations for insulin delivery to the respiratory tract. *Int J Nanomed*. 2024;19:9195–9211. doi:10.2147/IJN.S474287
43. Liu J, Leng P, Liu Y. Oral drug delivery with nanoparticles into the gastrointestinal mucosa. *Fundam Clin Pharmacol*. 2021;1:86–96. doi:10.1111/fcp.12594
44. Lozoya-Agullo I, Zur M, Wolk O, et al. In-situ intestinal rat perfusions for human Fabs prediction and BCS permeability class determination: investigation of the single-pass vs. the Doluisio experimental approaches. *Int J Pharm*. 2015;1-2:1–7.
45. Yao Y, Mi W, Cao G, et al. The absorption characteristics of nonvolatile components in a water extraction from amomi fructus as determined by in situ single-pass intestinal perfusion and high-performance liquid chromatography. *Front Pharmacol*. 2020;11:711. doi:10.3389/fphar.2020.00711
46. Selyutina OY, Polyakov NE. Glycyrrhizic acid as a multifunctional drug carrier – from physicochemical properties to biomedical applications: a modern insight on the ancient drug. *Int J Pharm*. 2019;559:271–279.
47. Zheng B, Liu DY, Qin XW, et al. Mucoadhesive-to-mucopenetrating nanoparticles for mucosal drug delivery: a mini review. *Int J Nanomed*. 2025;20:2241–2252.
48. He YJ, Cheng M, Yang RY, et al. Research progress on the mechanism of nanoparticles crossing the intestinal epithelial cell membrane. *Pharmaceutics*. 2023;7:1816. doi:10.3390/pharmaceutics15071816
49. Wang Y, Mo YL, Sun YW, et al. Intestinal nanoparticle delivery and cellular response: a review of the bidirectional nanoparticle-cell interplay in mucosa based on physiochemical properties. *J Nanobiotechnology*. 2024;1:669. doi:10.1186/s12951-024-02930-6
50. Shen CY, Yang YQ, Shen BD, et al. Self-discriminating fluorescent hybrid nanocrystals: efficient and accurate tracking of translocation via oral delivery. *Nanoscale*. 2017;1:436–450.
51. Nakamura Y, Kimura S, Hase K. M cell-dependent antigen uptake on follicle-associated epithelium for mucosal immune surveillance. *Inflamm Regen*. 2018;38:15. doi:10.1186/s41232-018-0072-y
52. Castillo DD, Lo DD. Deciphering the M-cell niche: insights from mouse models on how microfold cells "know" where they are needed. *Front Immunol*. 2024;15:1400739. doi:10.3389/fimmu.2024.1400739
53. Liu ZQ, Jiang ZH, Liu L, et al. Mechanisms responsible for poor oral bioavailability of paeoniflorin: role of intestinal disposition and interactions with sinomenine. *Pharm Res*. 2006;12:2768–2780. doi:10.1007/s11095-006-9100-8
54. Shen CY. Study on the identification of self-assembled nanoparticles from Shaoyao Gancao Decoction and its effect on compatibility. Master's Thesis, Chengdu University of Traditional Chinese Medicine, 2021.